Acta Crystallographica Section D
Biological Crystallography
ISSN 0907-4449

Structures of ternary complexes of aspartate-semialdehyde dehydrogenase (Rv3708c) from *Mycobacterium tuberculosis* H37Rv

Rajan Vyas,[a] Rupinder Tewari,[a] Manfred S. Weiss[b]‡ and Subramanian Karthikeyan[c]*

[a]Department of Biotechnology, Panjab University, Chandigarh 160 014, India, [b]EMBL Hamburg Outstation, c/o DESY, Notkestrasse 85, D-22603 Hamburg, Germany, and [c]Institute of Microbial Technology, Council of Scientific and Industrial Research (CSIR), Sector 39-A, Chandigarh 160 036, India

‡ Current address: Helmholtz-Zentrum Berlin für Materialien und Energie, Macromolecular Crystallography (HZB-MX), Albert-Einstein-Strasse 15, D-12489 Berlin, Germany.

Correspondence e-mail: skarthik@imtech.res.in

Received 26 November 2011
Accepted 18 February 2012

PDB References: aspartate-semialdehyde dehydrogenase, complex with SMCS and sulfate, 3tz6; complex with glycerol and sulfate, 3vos.

Aspartate-semialdehyde dehydrogenase (Asd; ASADH; EC 1.2.1.11) is the enzyme that lies at the first branch point in the biosynthetic pathway of important amino acids including lysine and methionine and the cell-wall component diaminopimelate (DAP). The enzymatic reaction of ASADH is the reductive dephosphorylation of aspartyl-β-phosphate (ABP) to aspartate β-semialdehyde (ASA). Since the aspartate pathway is absolutely essential for the survival of many microbes and is absent in humans, the enzymes involved in this pathway can be considered to be potential antibacterial drug targets. In this work, the structure of ASADH from *Mycobacterium tuberculosis* H37Rv (*Mtb*-ASADH) has been determined in complex with glycerol and sulfate at 2.18 Å resolution and in complex with *S*-methyl-L-cysteine sulfoxide (SMCS) and sulfate at 1.95 Å resolution. The overall structure of *Mtb*-ASADH is similar to those of its orthologues. However, in the *Mtb*-ASADH–glycerol complex structure the glycerol molecule is noncovalently bound to the active-site residue Cys130, while in the *Mtb*-ASADH–SMCS complex structure the SMCS (Cys) is covalently linked to Cys130. The *Mtb*-ASADH–SMCS complex structurally mimics one of the intermediate steps in the proposed mechanism of ASADH enzyme catalysis. Comparison of the two complex structures revealed that the amino acids Glu224 and Arg249 undergo conformational changes upon binding of glycerol. Moreover, the structures reported here may help in the development of species-specific antibacterial drug molecules against human pathogens.

1. Introduction

Tuberculosis (TB), one of the most contagious diseases, claims close to three million lives annually. Every second, someone in the world becomes newly infected with *Mycobacterium tuberculosis* (*Mtb*), the causative agent of TB (http://www.tballiance.org). TB had been thought to be under control until three decades ago, and its re-emergence has raised serious alarm all over the world. The main reasons for the persistence of *Mtb* as a global killer are the development of resistant strains against the existing antibiotics (isoniazid, rifampin, ethambutol and streptomycin) and the lengthy treatment of about 6–9 months (Besra & Kremer, 2002), which can be difficult for patients to complete. Consequently, more and more drug-resistant strains of *Mtb* such as XDR (extensively drug-resistant) and MDR (multi-drug-resistant), which are hard to treat using the present drug therapy, are emerging (Jain & Dixit, 2008). Therefore, there is an urgent need to develop a new class of drugs against *Mtb* which would reduce

the duration of treatment and show activity against drug-resistant strains. The design of inhibitors by targeting the essential enzymes of *Mtb* is an upcoming approach against the growing threat of tuberculosis. The enzyme aspartate-β-semialdehyde dehydrogenase (ASADH) encoded by the *asd* gene is involved in the aspartate metabolic pathway and has been shown to be essential in *Mtb* (Cirillo *et al.*, 1994). Knockout strains as well as perturbations to the *asd* gene have been reported to be lethal in *Legionella pneumophila* (Harb & Kwaik, 1998), *Salmonella typhimurium* (Galán *et al.*, 1990) and *Streptococcus mutans* (Cardineau & Curtiss, 1987) owing to the fact that the strains are auxotrophic for the crucial cell-wall component diaminopimelate (DAP), an intermediate metabolite in the aspartate pathway. Since DAP is not required in mammals and the complete aspartate pathway is absent in mammals, the enzymes involved in this pathway are valid as potential drug targets.

The first step in the aspartate pathway is the phosphorylation of aspartic acid to form L-β-aspartyl-phosphate (ABP) catalyzed by the enzyme aspartate kinase (ASK; Cohen, 1985). L-β-Aspartyl-phosphate (ABP) is further reductively dephosphorylated to L-aspartate β-semialdehyde (ASA) by the enzyme aspartate-β-semialdehyde dehydrogenase (ASADH; Fig. 1). ASA can be further utilized either in the synthesis of DAP and lysine by dihydrodipicolinate synthase (lysine biosynthetic pathway) or by homoserine dehydrogenase to synthesize methionine, threonine and isoleucine (homoserine biosynthetic pathway) (Gerdes *et al.*, 2003; Viola, 2001).

ASADH physiologically converts L-aspartyl-β-phosphate (ABP) to L-aspartate β-semialdehyde (ASA) in the presence of reduced nicotinamide adenine dinucleotide phosphate (NADPH). The complete chemical mechanism of ASADH is now well understood based on many structural, mutational and chemical modification studies (Blanco, Moore, Kabaleeswaran *et al.*, 2003; Blanco *et al.*, 2003; Karsten & Viola, 1991, 1992; Ouyang & Viola, 1995). Studies of the modification of the active-site cysteine with several thiol-specific reagents and substrate-analogue thiols such as *S*-methyl-L-cysteine sulfoxide (SMCS), which inhibits the activity of ASADH by forming a covalent disulfide bond to the active-site Cys, confirmed the role of the cysteine residue in catalysis (Karsten & Viola, 1992; Hadfield *et al.*, 2001; Blanco, Moore, Kabaleeswaran *et al.*, 2003). Moreover, L-β-aspartyl-phosphate (substrate) analogues such as methylene phosphonate, difluoromethylene phosphonate, phosphoramidate, cyclic phosphonate and unsaturated and fluorinated analogues have also been shown to inhibit the ASADH enzyme at micromolar concentrations (Cox *et al.*, 2001, 2002, 2005; Adams *et al.*, 2002; Evitt & Cox, 2011). Recently, several inhibitors have been identified through small-molecule fragment-library screening and have been structurally characterized with ASADH from *Streptomyces pneumoniae* and *Vibrio cholerae* (Pavlovsky *et al.*, 2012).

In all microbes, the oligomeric state of functional ASADH has been observed to be a homodimer (Hadfield *et al.*, 2001; Blanco, Moore, Kabaleeswaran *et al.*, 2003; Blanco, Moore & Viola, 2003). The structure of the ASADH monomer is comprised of an N-terminal nucleotide-binding domain and a C-terminal dimerization domain. The N-terminal domain constitutes an approximate Rossmann fold and the first β-strand (β1) of the N-terminal domain contributes to a glycine-rich loop which is characteristic of an NADP-binding domain. The C-terminal domain is responsible for dimerization of the enzyme and provides residues responsible for binding of the substrate and catalysis (Hadfield *et al.*, 1999, 2001).

Crystal structures of ASADHs from *Escherichia coli* (*Ec*-ASADH; Ouyang & Viola, 1995; Hadfield *et al.*, 1999, 2001), *Haemophilus influenzae* (*Hi*-ASADH; Blanco, Moore & Viola, 2003; Blanco, Moore, Faehnle & Viola, 2004; Blanco, Moore, Faehnle, Coe *et al.*, 2004; Faehnle *et al.*, 2004), *V. cholerae* (isoform I, *Vc*-ASADH1, Blanco, Moore, Kabaleeswaran *et al.*, 2003; isoform II, *Vc*-ASADH2, Viola *et al.*, 2008), *S. pneumoniae* (*Sp*-ASADH; Faehnle *et al.*, 2006), *Methanococcus jannaschii* (*Mj*-ASADH; Faehnle *et al.*, 2005) and *Candida albicans* (*Ca*-ASADH; Arachea *et al.*, 2010) have been reported. In addition, a model has been predicted for *Mtb*-ASADH based on homology-modelling studies (Singh *et al.*, 2008). In all structurally known ASADHs the catalytic residues are highly conserved, which suggests that catalysis proceeds in a similar manner. Despite this apparent mechanistic conservation, there is a drastic difference in catalytic efficiency among enzymes from Gram-negative (Moore *et al.*, 2002), Gram-positive (Faehnle *et al.*, 2006) and archaeal (Faehnle *et al.*, 2005) bacteria. It has been suggested that the observed difference in catalytic efficiency may be a consequence of the low degree of sequence identity and differences in several secondary-structural elements that are missing or truncated in all bacterial ASADH family members compared with Gram-negative ASADHs (Faehnle *et al.*, 2005, 2006). Also, the residues that form critical interactions with NADP in Gram-negative bacterial ASADHs are not conserved in Gram-positive and archaeal ASADHs. These local alterations have been suggested to play an important role in the binding and release of $NADP^+$, resulting in the differing catalytic efficiencies among the ASADH enzymes (Faehnle *et al.*, 2005, 2006). In addition, several crystal structures of complexes with substrate, cofactor and inhibitors have been studied in order to highlight the active-site organization and to

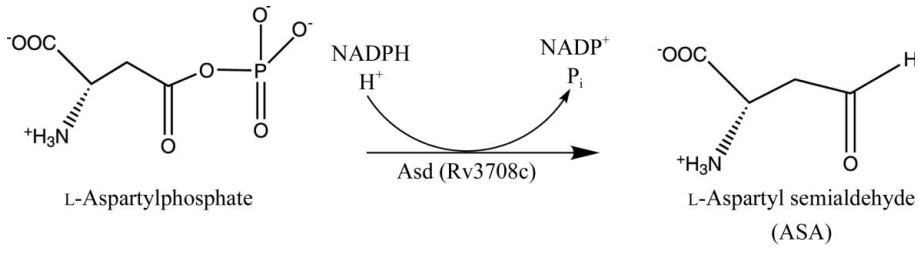

Figure 1
The reaction catalysed by ASADH.

Table 1
Data-collection and refinement statistics for *Mtb*-ASADH.

Values in parentheses are for the last shell.

	Glycerol–SO_4	SMCS (Cys)–SO_4
Data-collection statistics		
Wavelength (Å)	1.067	1.542
Resolution range (Å)	99.00–2.18 (2.22–2.18)	50.00–1.95 (2.02–1.95)
Space group	*F*432	*F*432
Unit-cell parameters (Å)	$a = b = c = 267.37$	$a = b = c = 266.16$
Mosaicity (°)	0.47	0.34
Total No. of reflections	352300	335069
Unique reflections	43078	58651
Multiplicity	8.2 (7.5)	5.7 (4.9)
$\langle I/\sigma(I)\rangle$	14.1 (2.2)	19.4 (2.2)
Completeness (%)	99.9 (100.0)	99.4 (99.5)
$R_{\rm merge}$† (%)	15.5 (94.7)	7.5 (72.8)
Refinement statistics		
Resolution range (Å)	32.42–2.18	29.21–1.95
Unique reflections	43066	58293
Completeness (%)	99.9	98.8
$R_{\rm cryst}$‡	0.181	0.192
$R_{\rm free}$§	0.194	0.211
R.m.s.d. values		
Bond lengths (Å)	0.007	0.008
Bond angles (°)	1.2	1.3
Ramachandran plot		
Most favoured (%)	90.0	90.6
Additionally allowed (%)	8.9	8.0
Generously allowed (%)	1.1	1.4
Mtb-ASADH model		
No. of modelled residues	338	343
No. of glycerol molecules	3	3
No. of sulfate ions	6	6
No. of water molecules	339	368
Average *B*-factor values (Å^2)		
Protein	29.2	29.2
Ligand	40.3 [glycerol]	37.7 [Cys]
Glycerol	43.5	49.7
Sulfate ions	38.9	43.7
Water	41.0	43.5
PDB code	3vos	3tz6

† $R_{\rm merge} = \sum_{hkl}\sum_i |I_i(hkl) - \langle I(hkl)\rangle|/\sum_{hkl}\sum_i I_i(hkl)$, where $I(hkl)$ is the intensity of reflection hkl. ‡ $R_{\rm cryst} = \sum_{hkl} ||F_{\rm obs}| - |F_{\rm calc}||/\sum_{hkl}|F_{\rm obs}|$. § $R_{\rm free}$ is the cross-validation R factor computed for a test set consisting of 5% of the reflections.

understand the molecular mechanism of ASADH enzymes. Structures complexed with substrates to represent intermediate states in enzyme catalysis have been reported for *Hi*-ASADH (Blanco, Moore & Viola, 2003). Despite the availability of crystal structures of ASADH from different organisms, the structure of ASADH from one of the most pathogenic organisms, *Mtb*, has remained elusive. The ASADH amino-acid sequences exhibit a similarity of about 40–60% between the various bacterial species. Here, we report two crystal structures of *Mtb*-ASADH, the first bound with glycerol and sulfate and the second complexed with a substrate analogue (SMCS) and sulfate.

2. Materials and methods

2.1. Cloning, expression and purification of the *Mtb*-ASADH enzyme

The *asd* gene of *Mtb* was cloned in the pGEM-T Easy vector, subcloned into the expression vector pQE30 (pSST1) and overexpressed in *E. coli* M15 strain (Shafiani *et al.*, 2005). Soluble expression and purification of the recombinant *Mtb*-ASADH protein was achieved using an optimized expression and purification protocol (Vyas *et al.*, 2008). The optimized conditions included lowering the pre-induction temperature (from 310 to 288 K), induction of the culture using 0.05 m*M* IPTG at 288 K and a post-induction incubation for 18 h at 288 K. The expressed protein was purified using Ni–NTA affinity chromatography followed by size-exclusion chromatography (Vyas *et al.*, 2008).

2.2. Crystallization, data collection and data processing

Crystals of *Mtb*-ASADH were grown as described previously (Vyas *et al.*, 2008). Briefly, purified *Mtb*-ASADH (concentration 9 mg ml^{-1}) in 10 m*M* potassium phosphate buffer pH 8.0 and 10 m*M* DTT was screened for crystallization using the sitting-drop vapour-diffusion method. Cubic crystals were obtained when *Mtb*-ASADH was equilibrated against a reservoir buffer composed of 1.6 *M* ammonium sulfate and 100 m*M* citric acid pH 5.0. For diffraction data collection, crystals were treated with 27%(*v*/*v*) glycerol in reservoir buffer for 30 s and flash-cooled to 100 K. Diffraction data were collected to 2.18 Å resolution on the BM14 beamline at the ESRF, Grenoble, France using a MAR Mosaic (225 mm) CCD detector and were integrated using *DENZO* and *SCALEPACK* (Otwinowski & Minor, 1997). To obtain the SMCS (Cys) complex, crystals were incubated with 5 m*M* SMCS overnight. Diffraction data were collected to 1.95 Å resolution using a MAR 345 image-plate detector mounted on a Rigaku MicroMax-007 HF X-ray generator equipped with Osmic Varimax optics. The SMCS complex data were indexed, integrated and scaled using *HKL*-2000 (Otwinowski & Minor, 1997). For both data sets, intensities were converted to structure-factor amplitudes using the program *TRUNCATE* (French & Wilson, 1978) as implemented in *CCP*4 (Winn *et al.*, 2011). Data-collection and processing statistics are given in Table 1.

2.3. Structure determination and refinement of the *Mtb*-ASADH structure

The structure of *Mtb*-ASADH was solved by the molecular-replacement method using *Sp*-ASADH (38% identity and 56% similarity to *Mtb*-ASADH; PDB entry 2gyy; Faehnle *et al.*, 2006) as a starting model in the program *AMoRE* (Navaza, 2001). The highest peaks in the rotation function and translation function were 7.9σ and 6.0σ, respectively. The orientation and position were further refined using rigid-body refinement in the resolution range 10.0–4.0 Å. The final correlation coefficient for the top solution was 0.48, with an *R* factor of 40.3%. The model was refined using *REFMAC*5 (Murshudov *et al.*, 2011). During refinement, 5% of the reflections were kept aside and used for calculation of the free *R* factor. Electron density was calculated using the refined model by fast Fourier transform and the model was built manually using *Coot* (Emsley & Cowtan, 2004). Refinement and model building were performed repeatedly for several cycles until no further reduction in *R* and $R_{\rm free}$ was observed.

The final model was validated using *PROCHECK* (Laskowski *et al.*, 1993).

3. Results and discussion

3.1. Quality of the model

The *Mtb*-ASADH structure was solved in the cubic space group *F*432 by molecular replacement using *Sp*-ASADH (PDB entry 2gyy; Faehnle *et al.*, 2006) as a search model. The structure was then refined against data extending to 2.18 Å resolution. The resulting final Fourier map of the *Mtb*-ASADH structure was of good quality and allowed modelling of 338 out of 345 residues. The NADP-binding loop (residues 39–42) and the C-terminal residues 343–345 could not be traced in the electron-density map and were not included in the model. In addition, a seven-residue loop (25–31) was built with an occupancy of 0.8 owing to its flexibility. In the active-site region of *Mtb*-ASADH electron density was observed at the 3.0σ level in the difference Fourier map which could be modelled as a glycerol molecule (Fig. 2*a*), in addition to two other glycerol molecules which were bound at the surface. Furthermore, six sulfate ions were modelled in the difference Fourier map which were above the 3.0σ level, including one in the active-site region (Fig. 2*b*). Although at this resolution it is not possible to distinguish between phosphate ions and sulfate ions unambiguously, we have modelled these ions as sulfate ions as the *Mtb*-ASADH crystals were grown in the presence of 1.6 *M* ammonium sulfate. The final model thus consisted of 338 residues, six sulfate ions, three glycerol molecules and 339 water molecules, with R and $R_{\rm free}$ values of 18.1% and 19.4%, respectively. The final model showed that 90% of the amino-acid residues are in the most favoured region, 8.9% are in the additionally allowed region and 1.1% are in the generously allowed region of the Ramachandran plot as analyzed by *PROCHECK* (Laskowski *et al.*, 1993).

The *Mtb*-ASADH–SMCS complex structure was solved in the cubic space group *F*432 by rigid-body refinement using *Mtb*-ASADH as the starting model. The first residue at the N-terminus and the last two residues at the C-terminus could not be modelled owing to a lack of electron density and thus were not included in the final model. Residues 39–42

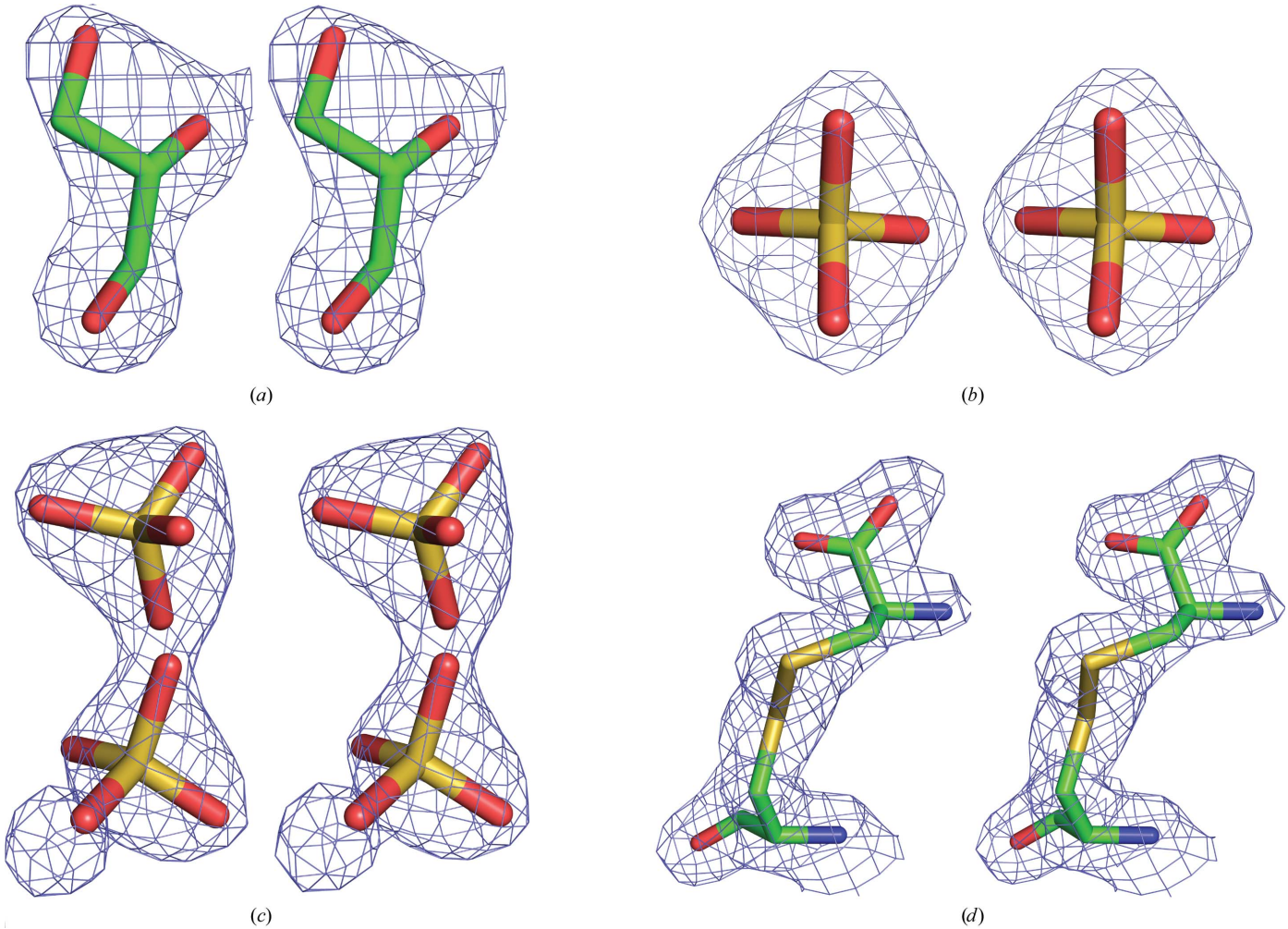

Figure 2
Stereoview showing the final ($2mF_{\rm o} - DF_{\rm c}$,$\alpha_{\rm c}$) electron-density map contoured at the 1.5σ level (*a*) for glycerol, (*b*) for sulfate ion, (*c*) for sulfate ion with an alternate conformation and (*d*) for the covalent adduct with cysteine (SMCS).

corresponding to the NADP-binding loop showed only weak electron density owing to the absence of NADP. However, the loop formed by residues 25–31 was ordered and could be modelled into the electron-density map and refined with full occupancy. The difference Fourier electron-density map in the active-site region showed extra electron density which was modelled as a cysteine residue forming a covalent adduct with the catalytic residue Cys130 (Fig. 2*d*). The final model consisted of 342 residues, one covalently linked Cys, six sulfate ions, three glycerol molecules and 368 water molecules, with R and $R_{\rm free}$ values of 19.2% and 21.1%, respectively. The final model showed that 90.6% of all amino-acid residues are in the most favoured region, 8.0% are in the additionally allowed region and 1.4% are in the generously allowed region of the Ramachandran plot as analyzed by *PROCHECK* (Laskowski *et al.*, 1993). The final data and refinement statistics are shown in Table 1.

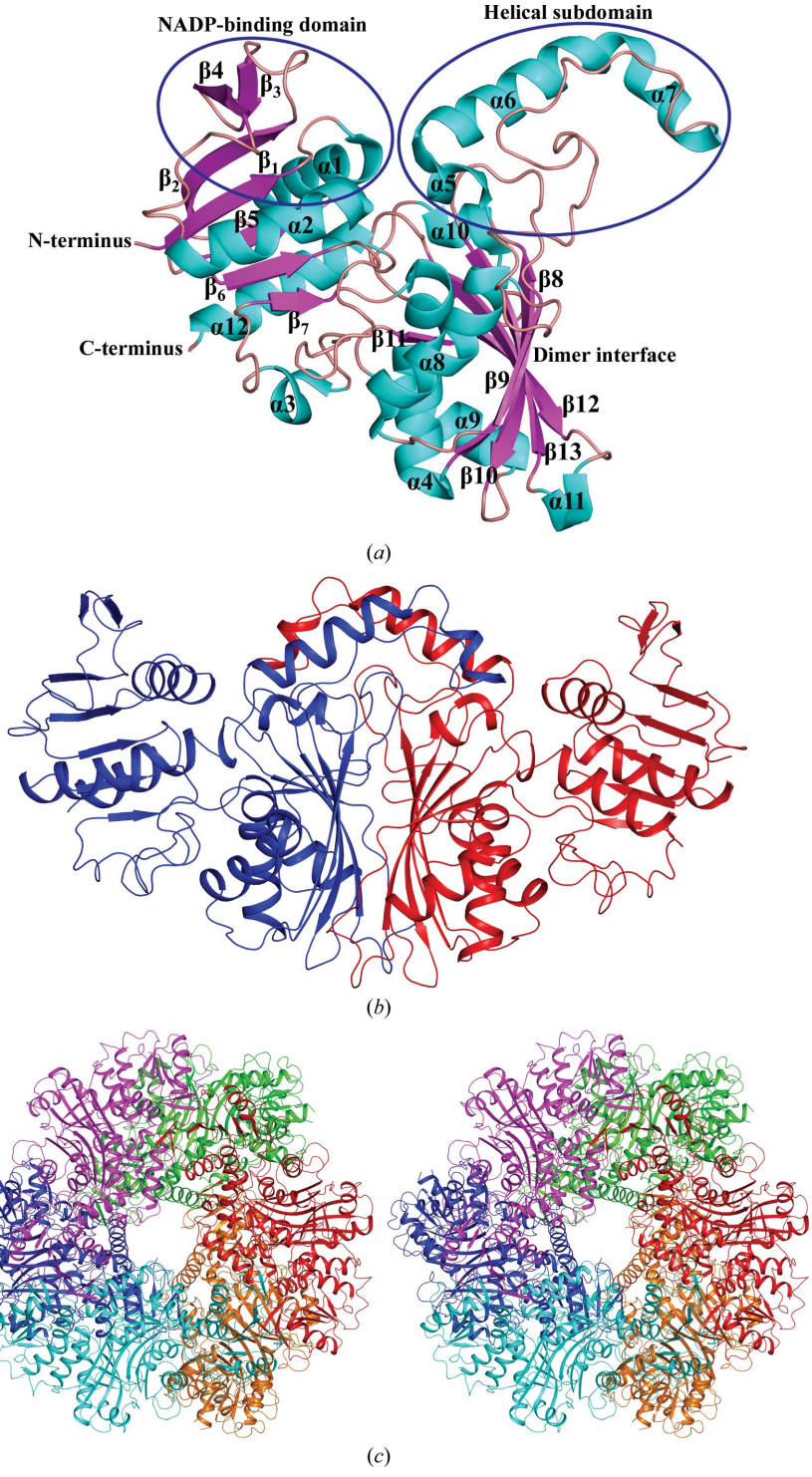

Figure 3
Mtb-ASADH structure. (*a*) Monomer with N- and C-termini, dimer interface, NADP-binding domain and helical subdomain labelled. (*b*) Cartoon representation of the *Mtb*-ASADH dimer created by applying crystallographic twofold symmetry (blue and red). (*c*) Cartoon representation of the dodecameric arrangement of *Mtb*-ASADH, with each dimer displayed in a single colour. All figures were generated using *PyMOL* (v.1.2r3pre; Schrodinger LLC).

3.2. Overall three-dimensional structure of *Mtb*-ASADH

Similar to other known ASADH structures, the *Mtb*-ASADH monomer (Fig. 3*a*) is built up of an N-terminal nucleotide-binding domain (residues 1–129 and 330–342) and a C-terminal catalytic and dimerization domain (residues 130–329). The *Mtb*-ASADH structure consists of a total of 12 α-helices and 13 β-strands arranged in two β-sheets. The architecture of the N-terminal domain is comprised of α-helices and β-sheets (β1–β7, α1–α2 and α12) forming an approximate Rossmann fold characteristic of an NADP-binding domain. The C-terminal domain (β8–β13 and α3–α11) is responsible for dimerization and forms a dimer interface with a six-stranded β-sheet facing towards the opposite subunit of the dimer and provides catalytic residues as in other ASADH family members (Hadfield *et al.*, 1999, 2001).

The structure of *Mtb*-ASADH was solved in the cubic space group $F432$ with one monomer per asymmetric unit and shows a $V_{\rm M}$ value (Matthews coefficient; Matthews, 1968) of 5.24 Å^3 Da^{-1} and 76.5% solvent content. The functional form of *Mtb*-ASADH has been reported to be a dimer (Vyas *et al.*, 2008). In the crystal, the dimer is formed by applying crystallographic twofold rotational symmetry to the monomer (Fig. 3*b*). The interactions between the monomers in a dimer are mainly mediated through its dimerization domain, with hydrogen-bonding contacts formed between residues Arg150, Arg175, Gly188, Asn206, Gly220, Asp225, Ser244, Gly245 and Thr246

from one subunit and residues Asp308, Glu182, Ala295, Leu292, Arg304, Asn261 and Arg306 of the other subunit. Moreover, analysis of the crystal packing (Fig. 3*c*) shows that 12 subunits assemble to form a dodecamer. An analysis of the accessible surface area of *Mtb*-ASADH using the *PISA* (*Protein Interactions, Surfaces and Assemblies*) server (Krissinel & Henrick, 2007) indicates that the buried surface area for a dimer is about 2850 Å^2 (20% of the total accessible area), while it is only 647 Å^2 (2.9% of the total accessible area) between the dimers in the dodecameric assembly. Since the contacts between dimers are made up of only a few interactions, we conclude that the preferred oligomeric form of *Mtb*-ASADH in solution is a dimer.

3.3. Active site of *Mtb*-ASADH with glycerol and sulfate ion (*Mtb*-ASADH–glycerol–SO_4)

Mtb-ASADH was initially crystallized and the structure was solved as the native protein. However, after refinement of the structure a difference Fourier map at the 3.0σ level showed electron density near the active-site residue Cys130 which could be modelled as glycerol (Fig. 2*a*). In addition, two further glycerol molecules were also bound to *Mtb*-ASADH. These glycerol molecules might be contributed from the cryoprotectant solution [27%(*v*/*v*) glycerol] that was used to protect the crystals during flash-cooling to 100 K for data collection. The glycerol molecule bound at the active site is anchored in position through hydrogen bonding of its O1 atom to Cys130 SG, to His256 NE2 and to O4 of the sulfate ion through a water molecule (Fig. 4*a*). Similarly, the O2 atom of glycerol interacts with the guanidinium N atoms of Arg249 and with the O atom of Ala158 through a water molecule. The O3 atom of glycerol also interacts with Glu224 OE2 and Ser162 OG through a water molecule. The second glycerol molecule is bound at the dimeric interface of *Mtb*-ASADH and interacts with the O atom of Gly188 and the N atom of Phe193 through a solvent molecule. The third glycerol molecule is bound at the surface and interacts with the guanidinium N atom NH1 of Arg229. Moreover, the difference Fourier map showed electron density near to the active site and at the surface regions which was modelled as sulfate ions. The sulfate ion bound at the active site is anchored in position through hydrogen bonding of O1 to Cys130 N, of O2 to Gly161 O through a water molecule, of O3 to Arg99 NH2 and of O4 to Asn129 ND2, Arg99 NH1 and Lys227 NZ (Fig. 4*a*). Superposition of *Hi*-ASADH (Blanco, Moore & Viola, 2003) with *Mtb*-ASADH revealed that the sulfate ion in *Mtb*-ASADH occupies a similar position to that occupied by a phosphate ion in *Hi*-ASADH. In addition, one of the sulfate ions was refined with two conformations in the NADP-binding domain. The remainder of the sulfate ions were bound at the surface of *Mtb*-ASADH and interact with Arg43, Arg120, Arg233 and Arg274.

3.4. Active site of *Mtb*-ASADH with SMCS and sulfate ion (*Mtb*-ASADH–SMCS–SO_4)

SMCS is a substrate analogue of ASA and is thought to be a competitive inhibitor of ASADH (Karsten & Viola, 1991). Previous studies showed that the incubation of SMCS with ASADH leads to the formation of a complex in which SMCS is converted into cysteine owing to reductive demethylation and that the resulting cysteine interacts covalently with the catalytic site residue Cys130 of ASADH (Hadfield *et al.*, 2001; Blanco, Moore, Kabaleeswaran *et al.*, 2003). In order to investigate the interaction of *Mtb*-ASADH with SMCS and to explore whether it could be a potential inhibitor, *Mtb*-ASADH crystals were soaked overnight in 5 m*M* SMCS. Diffraction data to 1.95 Å resolution were then collected from the SMCS-soaked crystal and the structure was determined. The difference Fourier electron-density map of the *Mtb*-ASADH–SMCS complex clearly showed continuous electron density at the catalytic residue Cys130 which could be modelled as a cysteine residue. The Cys residue makes a covalent bond with the catalytic residue Cys130 and occupies a similar position as in the *Vc*-ASADH–SMCS complex (Fig. 4*b*; Blanco, Moore, Kabaleeswaran *et al.*, 2003). The carboxyl group of SMCS is engaged in a bidentate interaction with the guanidinium N atoms of Arg249 and the NE2 atom of His256. Moreover, the Glu224 side chain was refined in two alternate conformations,

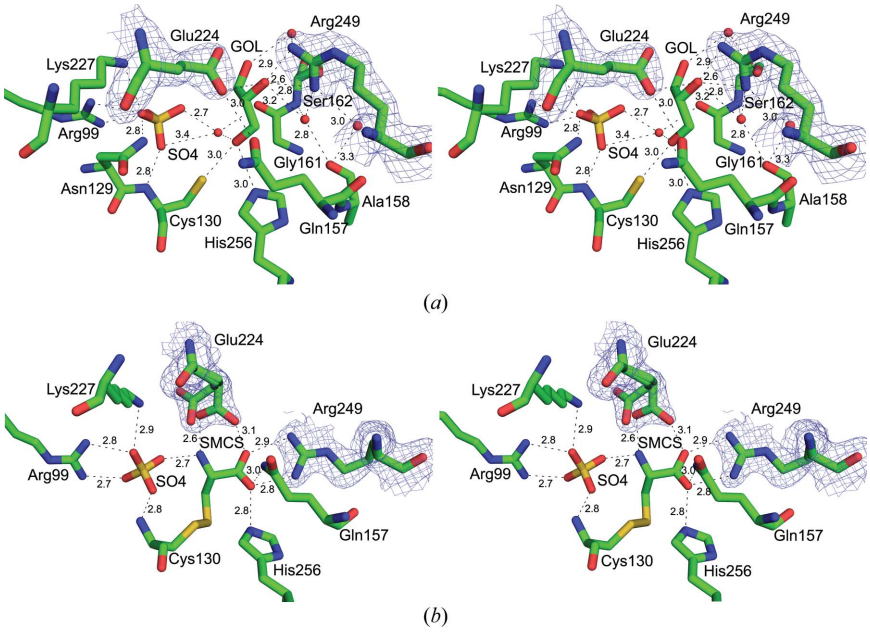

Figure 4
(*a*) Stereoview of the active site of the *Mtb*-ASADH–glycerol complex. The dashed line shows the interactions between glycerol and the residues of *Mtb*-ASADH. Water molecules are shown as red spheres. (*b*) Stereoview showing the covalent binding of SMCS (Cys) inhibitor to the active-site residue Cys130 of *Mtb*-ASADH. The dashed line shows the interactions between SMCS (Cys) and the interacting residues of *Mtb*-ASADH.

each with half occupancy. In one of the conformations of Glu224, OE1 and OE2 interact with the O and N atoms of SMCS, respectively (Fig. 4*b*). A sulfate ion occupies an identical position to a conserved phosphate group (Blanco, Moore & Viola, 2003), a byproduct of ASADH catalysis, at the active site and interacts with the N atom of SMCS, Lys227 NZ, Arg99 NH1 and NH2 and Cys130 N. Thus, this structure reveals the interactions of *Mtb*-ASADH in the presence of both SMCS (Cys) and a sulfate ion.

3.5. NADP-binding domain

In both the *Mtb*-ASADH–glycerol and the *Mtb*-ASADH–SMCS complex structures, the difference Fourier map consistently showed electron density in the NADP-binding domain which was modelled as two sulfate ions, each with half occupancy. The O atoms of the sulfate ions are at a hydrogen-bonding distance from Gln13, Gly163 and Leu164. Superposition of the NADP-complex structures of *Ec*-ASADH (PDB entry 1gl3; Hadfield *et al.*, 2001), *Vc*-ASADH1 (PDB entry 1mb4; Blanco, Moore, Kabaleeswaran *et al.*, 2003), *Hi*-ASADH (PDB entry 1pqu; Blanco, Moore, Faehnle & Viola, 2004), *Sp*-ASADH (PDB entry 2gz1; Faehnle *et al.*, 2006) and *Mj*-ASADH (PDB entry 1ys4; Faehnle *et al.*, 2005) onto the *Mtb*-ASADH structure revealed that the two sulfate ions occupy a similar position to the diphosphate moiety of NADP in all other structures. Previous studies have revealed that the conformations of NADP in ASADHs from Gram-positive bacteria (*Sp*-ASADH) and archaeal bacteria (*Mj*-ASADH) differ from those in ASADHs from Gram-negative bacteria (*Vc*-ASADH1 and *Ec*-ASADH; Blanco, Moore, Kabaleeswaran *et al.*, 2003; Hadfield *et al.*, 2001). Comparison of the *Mtb*-ASADH amino-acid sequence with those of other ASADHs shows that it exhibits a high degree of sequence similarity to *Sp*-ASADH (38% identity and 56% similarity). Moreover, both are from Gram-positive bacteria, suggesting that the binding conformation of NADP in *Mtb*-ASADH will be similar to that observed in the *Sp*-ASADH–NADP structure. In fact, the catalytic efficiencies of *Mtb*-ASADH (Shafiani *et al.*, 2005), *Sp*-ASADH (Faehnle *et al.*, 2006) and *Mj*-ASADH (Faehnle *et al.*, 2005) have been shown to be similar, suggesting that there may be some similarities between these enzymes (Moore *et al.*, 2002). However, knowledge of the crystal structure of *Mtb*-ASADH complexed with NADP is required to understand the binding mode of NADP and its interaction with *Mtb*-ASADH.

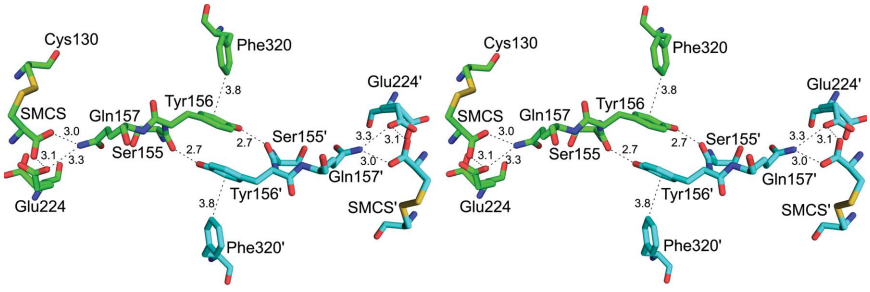

Figure 5
Inter-subunit contacts of *Mtb*-ASADH. The proposed tetrad residues of *Mtb*-ASADH connecting two active sites of the dimer are shown in green (one subunit) and cyan (the other subunit). The interactions are shown as dashed lines.

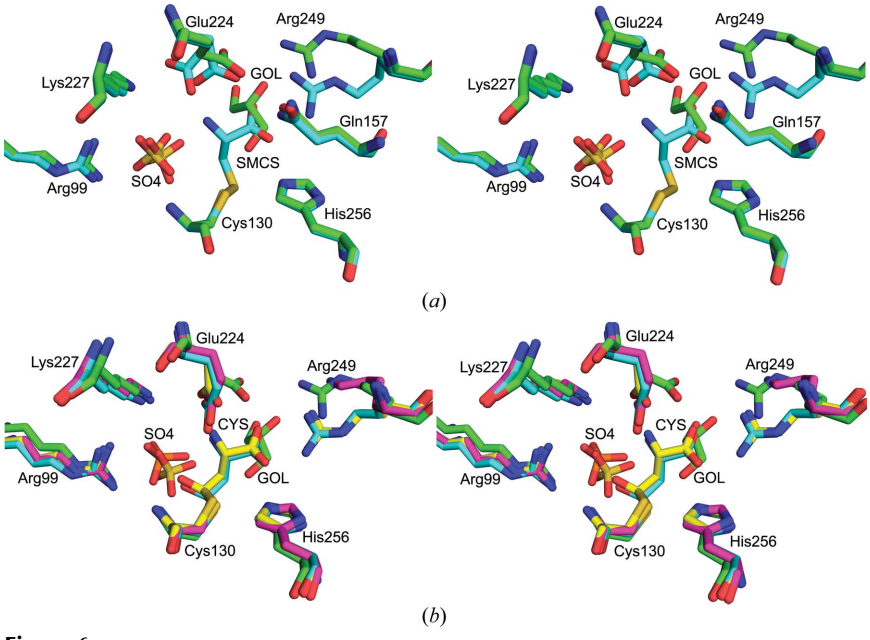

Figure 6
(*a*) Stereoview of the superposition of the *Mtb*-ASADH–SMCS (cyan) active site onto the *Mtb*-ASADH–glycerol (green) active site. (*b*) Stereoview of the superposition of the active sites of *Mtb*-ASADH–glycerol (green), native *Hi*-ASADH (cyan), *Hi*-ASADH R270K (purple) and *Hi*-ASADH E243D (yellow). The residues are numbered according to *Mtb*-ASADH.

3.6. Inter-subunit communication

In bacterial ASADH, a network of hydrophobic and hydrogen-bond interactions at the dimerization interface has been suggested to play a role in inter-subunit communication (Hadfield *et al.*, 2001; Blanco, Moore, Kabaleeswaran *et al.*, 2003; Nichols *et al.*, 2004) and supports the alternating-site or 'half-of-sites' reactivity model that has been proposed for the catalytic mechanism of ASADH (Biellmann *et al.*, 1980). In *Vc*-ASADH1, four residues, Thr160, Tyr161, Gln162 and Phe345, are projected to act as a signalling system through a hydrogen-bonding network that links the active sites of the two subunits (Blanco, Moore, Kabaleeswaran *et al.*, 2003). Notably, substitution of the Tyr residue in these four residues by either Leu or Met, as observed in fungal ASADHs, disrupted the network of hydrogen-bond

interactions and caused a loss of inter-subunit communication (Faehnle *et al.*, 2005; Arachea *et al.*, 2010). This has been proposed to play a role in the low catalytic activity of fungal ASADHs (Arachea *et al.*, 2010). In *Mtb*-ASADH all of the residues (Tyr156, Gln157 and Phe320 of *Mtb*-ASADH), with the exception of Thr160 (in *Vc*-ASADH), which was replaced by the similar residue Ser155 (in *Mtb*-ASADH), are conserved and may be involved in inter-subunit signalling by linking the two active sites through a network of hydrogen-bond interactions (Fig. 5); they may play a similar role as proposed in other bacterial species (Hadfield *et al.*, 2001; Blanco, Moore, Kabaleeswaran *et al.*, 2003; Nichols *et al.*, 2004).

3.7. Comparison of *Mtb*-ASADH with other ASADH structures

Superposition of *Mtb*-ASADH with other ASADH structures by *LSQMAN* (Kleywegt & Jones, 1995) showed root-mean-square deviations (r.m.s.d.s) of 1.9 Å (298 C^{α} atoms) with *Ec*-ASADH, 1.8 Å (301 C^{α} atoms) with *Vc*-ASADH1, 1.1 Å (323 C^{α} atoms) with *Vc*-ASADH2, 1.2 Å (313 C^{α} atoms) with *Sp*-ASADH, 1.5 Å (272 C^{α} atoms) with *Mj*-ASADH and 1.9 Å (295 C^{α} atoms) with *Hi*-ASADH, suggesting that the overall structure is similar in different species. Despite the high conservation of the overall structure and the active-site residues, the catalytic activity of ASADH varies from species to species, with k_{cat} values in the order Gram-negative > Gram-positive > fungal species (Moore *et al.*, 2002; Arachea *et al.*, 2010). The overall low sequence similarity throughout the family and the presence of insertions and deletions, especially in the cofactor-binding regions, were attributed to the observed differences in the catalytic efficiency among ASADHs (Faehnle *et al.*, 2006; Arachea *et al.*, 2010). Analysis of *Mtb*-ASADH in comparison to Gram-negative and fungal species shows that the length of the helical domain in *Mtb*-ASADH is longer than in fungal species but shorter than in Gram-negative bacteria and is consistent with the previous prediction that the length of the helical subdomain may play a role in enzyme catalysis (Faehnle *et al.*, 2006; Arachea *et al.*, 2010). *Mtb*-ASADH shows a high structural similarity to *Sp*-ASADH, with an r.m.s.d. of 1.2 Å for 313 C^{α} atoms; the enzymes have k_{cat} values of 8 s^{-1} (Shafiani *et al.*, 2005) and 2 s^{-1} (Faehnle *et al.*, 2006), respectively. *Mtb*-ASADH also shows high structural similarity to *Vc*-ASADH2, with an r.m.s.d. of 1.1 Å for 323 C^{α} atoms, which is also consistent with a previous prediction that the *Vc*-ASADH2 structure closely resembles those of ASADHs from Gram-positive bacteria and is likely to bind NADP in a similar manner, unlike *Vc*-ASADH1 (Viola *et al.*, 2008).

The *Mtb*-ASADH structure complexed with glycerol and cysteine superposes well, with an r.m.s.d. of 0.3 Å for 333 C^{α} atoms as calculated by *LSQMAN* (Kleywegt & Jones, 1995). However, a closer view of the active site of these complexes revealed a conformational change of residues Glu224 and Arg249 in glycerol-bound ASADH (Fig. 6*a*). Previous studies suggested that the orientation of the conserved Glu243 and Arg270 of *Hi*-ASADH (corresponding to Glu224 and Arg249 of *Mtb*-ASADH) are crucial for substrate binding and their mutants E243D and R270K exhibited drastically decreased catalytic efficiency (Blanco, Moore, Faehnle, Coe *et al.*, 2004). Interestingly, the conformation of Arg249 in the glycerol-bound *Mtb*-ASADH structure is similar to the conformation of lysine in the R270K mutant of *Hi*-ASADH, in which the orientation of lysine is 1.7 Å away from the terminal guanidine N atom of Arg270 (Fig. 6*b*; Blanco, Moore, Faehnle, Coe *et al.*, 2004). In the case of the *Hi*-ASADH E243D structure the mutation caused significant changes at the site of mutation and in the orientation of bound ASA (Blanco, Moore, Faehnle, Coe *et al.*, 2004). Although none of the observed structural changes were sufficient to account for the loss of activity, they are predicted to play a role in the enzyme-intermediate complex (Blanco, Moore, Faehnle, Coe *et al.*, 2004). Surprisingly, in the *Mtb*-ASADH–glycerol structure the Glu224 residue (Glu243 in *Hi*-ASADH) shows a significant conformational change by shifting away by 2.5 Å compared with its position in the *Mtb*-ASADH–SMCS complex (Fig. 6*a*). Although the catalytic activity of *Mtb*-ASADH is not affected by the presence of glycerol in *in vitro* studies (data not shown), the fact that it can induce conformational change of two important catalytic residues (Glu224 and Arg249) upon binding indicates that derivatives of glycerol could be potential inhibitors of *Mtb*-ASADH.

4. Conclusions

Mtb-ASADH is a potential drug target to combat TB. We have determined crystal structures of *Mtb*-ASADH in complex with glycerol and sulfate and in complex with SMCS and a sulfate ion. In the *Mtb*-ASADH–SMCS–SO_4 complex the SMCS (Cys) forms a covalent adduct with the catalytic residue (Cys130), mimicking the intermediate complex as proposed in the reaction mechanism (Karsten & Viola, 1991) and similar to that observed in the *Vc*-ASADH1–SMCS–NADPH complex structure (Blanco, Moore, Kabaleeswaran *et al.*, 2003). In addition, it also suggests that SMCS (Cys) or its derivatives could be used as a potential inhibitor, as the addition of Cys or SMCS to *Mtb*-ASADH abolishes enzymatic activity (Alvarez *et al.*, 2004; Karsten & Viola, 1991). In the *Mtb*-ASADH–glycerol–SO_4 complex the glycerol molecule was bound at the active site in a noncovalent form. The comparison of two structures of *Mtb*-ASADH revealed that the residues Glu224 and Arg249 undergo a conformational change upon glycerol binding which plays a role in catalysis by the enzyme. Based on our observations, we speculate that derivatives of glycerol may be potential lead compounds for the design of ASADH inhibitors. Moreover, the *Mtb*-ASADH structures reported here may be helpful in developing antibacterial drugs against this novel target.

We would like to thank the ESRF, Grenoble, France for the allocation and provision of synchrotron beam time at BM14. We also thank Dr Linda Schuldt (formerly of EMBL Hamburg, Germany and now at the University of Aarhus,

Denmark) for providing Fig. 1, the Department of Biotechnology, Government of India for financial support of this project and the Council of Scientific and Industrial Research (CSIR) for providing all infrastructure.

References

Adams, L. A., Cox, R. J., Gibson, J. S., Mayo-Martín, M. B., Walter, M. & Whittingham, W. (2002). *Chem. Commun.*, pp. 2004–2005.

Alvarez, E., Ramón, F., Magán, C. & Díez, E. (2004). *Biochim. Biophys. Acta*, **1696**, 23–29.

Arachea, B. T., Liu, X., Pavlovsky, A. G. & Viola, R. E. (2010). *Acta Cryst.* D**66**, 205–212.

Besra, G. S. & Kremer, L. S. (2002). *Expert Opin. Investig. Drugs*, **11**, 1033–1049.

Biellmann, J. F., Eid, P., Hirth, C. & Jörnvall, H. (1980). *Eur. J. Biochem.* **104**, 59–64.

Blanco, J., Moore, R. A., Faehnle, C. R., Coe, D. M. & Viola, R. E. (2004). *Acta Cryst.* D**60**, 1388–1395.

Blanco, J., Moore, R. A., Faehnle, C. R. & Viola, R. E. (2004). *Acta Cryst.* D**60**, 1808–1815.

Blanco, J., Moore, R. A., Kabaleeswaran, V. & Viola, R. E. (2003). *Protein Sci.* **12**, 27–33.

Blanco, J., Moore, R. A. & Viola, R. E. (2003). *Proc. Natl Acad. Sci. USA*, **100**, 12613–12617.

Cardineau, G. A. & Curtiss, R. (1987). *J. Biol. Chem.* **262**, 3344–3353.

Cirillo, J. D., Weisbrod, T. R., Pascopella, L., Bloom, B. R. & Jacobs, W. R. (1994). *Mol. Microbiol.* **11**, 629–639.

Cohen, G. N. (1985). *Methods Enzymol.* **113**, 596–599.

Cox, R. J., Gibson, J. S. & Hadfield, A. T. (2005). *Chembiochem*, **6**, 2255–2260.

Cox, R. J., Gibson, J. S. & Mayo Martín, M. B. (2002). *Chembiochem*, **3**, 874–886.

Cox, R. J., Hadfield, A. T. & Mayo-Martín, M. B. (2001). *Chem. Commun.*, pp. 1710–1711.

Emsley, P. & Cowtan, K. (2004). *Acta Cryst.* D**60**, 2126–2132.

Evitt, A. S. & Cox, R. J. (2011). *Mol. Biosyst.* **7**, 1564–1575.

Faehnle, C. R., Blanco, J. & Viola, R. E. (2004). *Acta Cryst.* D**60**, 2320–2324.

Faehnle, C. R., Le Coq, J., Liu, X. & Viola, R. E. (2006). *J. Biol. Chem.* **281**, 31031–31040.

Faehnle, C. R., Ohren, J. F. & Viola, R. E. (2005). *J. Mol. Biol.* **353**, 1055–1068.

French, S. & Wilson, K. (1978). *Acta Cryst.* A**34**, 517–525.

Galán, J. E., Nakayama, K. & Curtiss, R. (1990). *Gene*, **94**, 29–35.

Gerdes, S. Y. *et al.* (2003). *J. Bacteriol.* **185**, 5673–5684.

Hadfield, A., Kryger, G., Ouyang, J., Petsko, G. A., Ringe, D. & Viola, R. (1999). *J. Mol. Biol.* **289**, 991–1002.

Hadfield, A., Shammas, C., Kryger, G., Ringe, D., Petsko, G. A., Ouyang, J. & Viola, R. E. (2001). *Biochemistry*, **40**, 14475–14483.

Harb, O. S. & Abu Kwaik, Y. (1998). *Infect. Immun.* **66**, 1898–1903.

Jain, A. & Dixit, P. (2008). *J. Biosci.* **33**, 605–616.

Karsten, W. E. & Viola, R. E. (1991). *Biochim. Biophys. Acta*, **1077**, 209–219.

Karsten, W. E. & Viola, R. E. (1992). *Biochim. Biophys. Acta*, **1121**, 234–238.

Kleywegt, G. J. & Jones, T. A. (1995). *Structure*, **3**, 535–540.

Krissinel, E. & Henrick, K. (2007). *J. Mol. Biol.* **372**, 774–797.

Laskowski, R. A., MacArthur, M. W., Moss, D. S. & Thornton, J. M. (1993). *J. Appl. Cryst.* **26**, 283–291.

Matthews, B. W. (1968). *J. Mol. Biol.* **33**, 491–497.

Moore, R. A., Bocik, W. E. & Viola, R. E. (2002). *Protein Expr. Purif.* **25**, 189–194.

Murshudov, G. N., Skubák, P., Lebedev, A. A., Pannu, N. S., Steiner, R. A., Nicholls, R. A., Winn, M. D., Long, F. & Vagin, A. A. (2011). *Acta Cryst.* D**67**, 355–367.

Navaza, J. (2001). *Acta Cryst.* D**57**, 1367–1372.

Nichols, C. E., Dhaliwal, B., Lockyer, M., Hawkins, A. R. & Stammers, D. K. (2004). *J. Mol. Biol.* **341**, 797–806.

Otwinowski, Z. & Minor, W. (1997). *Methods Enzymol.* **276**, 307–326.

Ouyang, J. & Viola, R. E. (1995). *Biochemistry*, **34**, 6394–6399.

Pavlovsky, A. G., Liu, X., Faehnle, C. R., Potente, N. & Viola, R. E. (2012). *Chem. Biol. Drug Des.* **79**, 128–136.

Shafiani, S., Sharma, P., Vohra, R. M. & Tewari, R. (2005). *J. Appl. Microbiol.* **98**, 832–838.

Singh, A., Kushwaha, H. R. & Sharma, P. (2008). *J. Mol. Model.* **14**, 249–263.

Viola, R. E. (2001). *Acc. Chem. Res.* **34**, 339–349.

Viola, R. E., Liu, X., Ohren, J. F. & Faehnle, C. R. (2008). *Acta Cryst.* D**64**, 321–330.

Vyas, R., Kumar, V., Panjikar, S., Karthikeyan, S., Kishan, K. V. R., Tewari, R. & Weiss, M. S. (2008). *Acta Cryst.* F**64**, 167–170.

Winn, M. D. *et al.* (2011). *Acta Cryst.* D**67**, 235–242.